

A COMPARATIVE STUDY OF DISPLACED NON-KEPLERIAN ORBITS WITH IMPULSIVE AND CONTINUOUS THRUST

Jules Simo*

A study of novel families of highly non-Keplerian orbits (NKO) for spacecraft utilizing either solar sail or solar electric propulsion (SEP) at linear order are investigated in the circular restricted three-body problem (CRTBP). In addition to a detailed investigation of the dynamics and control of highly NKO, effort will be devoted to develop a strategy that uses maneuvers executed impulsively at discrete time intervals. Thus, impulse control is investigated as a means of generating displaced orbits. In order to compare the continuous thrust and impulse control orbits, linearized equations of motion will be considered for small displacements. The requirements for impulse control and continuous thrust for different values of out-of-plane distance are presented.

INTRODUCTION

The use of solar electric propulsion (SEP) technology becomes a realistic option for designing trajectories in interplanetary missions. The topics covered in this paper are the results of displaced periodic orbits in the Earth-Moon system in which the third body uses a hybrid solar sail. The hybrid sail model is composed conjointly with the two low thrust propulsion, namely a solar sail and a solar electric propulsion.

Also a solar sail is propelled by reflecting solar photons and therefore can transform the momentum of the photons into a propulsive force. Solar sailing technology appears as a promising form of advanced spacecraft propulsion, which can enable exciting new space-science mission concepts such as solar system exploration and deep space observation. Although solar sailing has been considered as a practical means of spacecraft propulsion only relatively recently, the fundamental ideas are by no means new (see McInnes¹). Solar sails can also be utilised for highly non-Keplerian orbits, such as closed orbits displaced high above the ecliptic plane (see Waters and McInnes²). Solar sails are especially suited for such non-Keplerian orbits, since they can apply a propulsive force continuously over indefinitely long periods, although only capable of very low thrust. This form of propulsion utilizes the pressure of sunlight and can provide energy changes greater than are possible with either ion or chemical propellants. This allows some exciting and unique trajectories (see Simo and McInnes^{3,4,5,6,7,8,9,10,11,12}). In such trajectories, a sail can be used as a communication satellite for high latitudes. For example, the orbital plane of the sail can be displaced above the orbital plane of the Earth, so that the sail can stay fixed above the Earth at some distance, if the orbital periods are equal. Orbits around the collinear points of the Earth-Moon system are also of great interest because their unique positions are advantageous for several important applications in space mission design (see e.g. Szebehely¹³, Roy,¹⁴ Vonbun,¹⁵ Thurman et al.,¹⁶ Gómez et al.^{17,18}).

*School of Engineering, University of Central Lancashire, Preston, PR1 1XJ, United Kingdom. Email: jsimo@uclan.ac.uk.

In the recent years several authors have tried to determine more accurate approximations (quasi-Halo orbits) of such equilibrium orbits¹⁹. The orbits were first studied by Farquhar²⁰, Farquhar and Kamel¹⁹, Breakwell and Brown²¹, Richardson²², Howell^{23,24}. Halo orbits near the collinear libration points in the Earth-Moon system are of great interest, particularly around the L_1 and L_2 points because their unique positions. However, a linear analysis shows that the collinear libration points L_1 , L_2 , and L_3 are of the type *saddle* \times *center* \times *center*, leading to the instability in their vicinity, whereas the equilateral equilibrium points L_4 , and L_5 are stable (*center* \times *center* \times *center*).

Due to the fact that the same face of the Moon always faces the Earth, a relay station is needed for communications with the far side of the Moon. Thus, Farquhar suggest to position one communications satellite in a halo orbit near the L_2 point.

If the orbit maintains visibility from Earth, a spacecraft on it (near the L_2 point) can be used to provide communications between the equatorial regions of the Earth and the lunar poles^{25,26,27}. Moreover, if another communications satellite is located at the L_1 point, there could be continuous communications coverage between the equatorial region of the Earth and the lunar surface.

The establishment of a bridge for radio communications is crucial for forthcoming space missions, which plan to use the lunar poles. McInnes²⁸ first investigated a new family of displaced solar sail orbits near the Earth-Moon libration points. In Baoyin and McInnes^{29,30,31} and McInnes^{28,32}, the authors describe the new orbits which are associated with artificial lagrange points in the Earth-Sun system. These artificial equilibria have potential applications for future space physics and Earth observation missions³³. In McInnes and Simmons³⁴, the authors investigate large new families of solar sail orbits, such as Sun-centered halo-type trajectories, with the sail executing a circular orbit of a chosen period above the ecliptic plane. In our study, we will demonstrate the possibility of such trajectories in the Earth-Moon system. As will be shown in the present study, there exist a new family of solar sail displaced periodic orbits in the Earth-Moon restricted three-body problem.

The first-order approximation is introduced for the linearized system of equations. The Laplace transform is used to produce the first-order analytic solution of the out-of plane motion. This paper investigates displaced periodic orbits at linear order in the circular restricted Earth- Moon system (CRTBP), where the third massless body utilizes a hybrid of solar sail and a solar electric propulsion (SEP). In particular, periodic motions in the vicinity of the Lagrange points in the Earth-Moon system will be explored along with their applications. The idea of combining a solar sail with an auxiliary system (SEP) to obtain a hybrid sail system is important especially due to the challenges of performing complex trajectories. The hybrid sail Earth-Moon system differs greatly from the Earth-Sun system as the Sun line direction varies continuously in the rotating frame and the equations of motion of the sail are given by a set of nonlinear non-autonomous ordinary differential equations. Firstly we describe the dynamic model of the hybrid sail. The study of the behaviour of dynamical system by means of appropriate feedback laws in control theory. Then, a feedback linearization control scheme is proposed and implemented. The main idea of this approach is to cancel the nonlinearities and to impose a desired dynamics. Nevertheless, the internal dynamics of the system is not always stable, therefore, we introduce a linear force opposing the velocity for damping the oscillations.

SYSTEM MODEL

In this work, we will assume that m_1 represents the larger primary (Earth), m_2 the smaller primary (Moon) and the motion of the hybrid sail which has a negligible mass will be considered. These

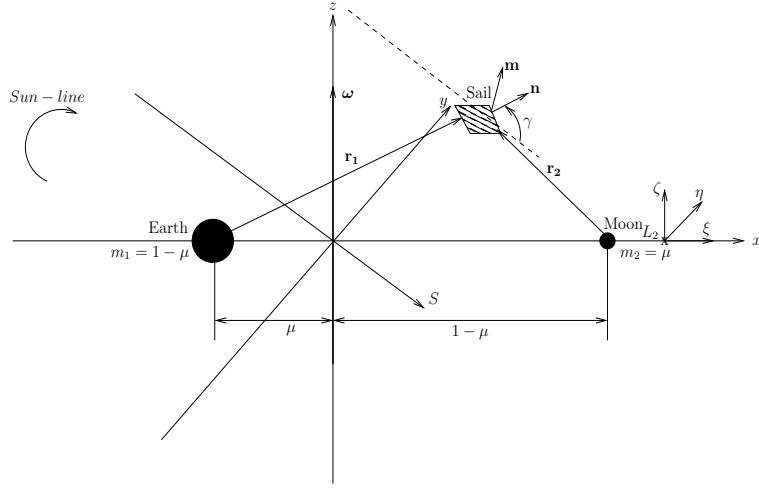


Figure 1 Schematic geometry of the Hybrid Sail in the Earth-Moon circular restricted three-body problem.

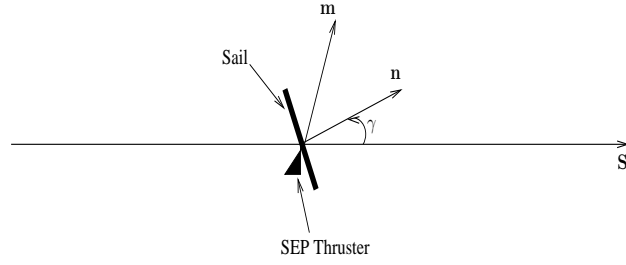


Figure 2 Angle γ between the Hybrid Sail surface normal \mathbf{n} and the Sun-line direction \mathbf{S} , and SEP thrust vector direction \mathbf{m} .

two massive bodies (primaries) are assumed to rotate about their common center of mass and the mass of the third body is too small to affect the motion of the two more massive bodies. The system is normalized such that the total mass ($m_1 + m_2$) is the unit mass, and the unit of length is the distance between the primaries. Thus, the orbital period of the system becomes 2π . The dashed line in Figure 1 is a line parallel to the Sun-line direction. The angle γ between the hybrid sail surface normal \mathbf{n} and the Sun-line direction \mathbf{S} can be seen in Figure 2.

Equations of Motions in Presence of the Hybrid Sail

The nondimensional equation of a motion of a hybrid sail in the rotating frame of reference is described by

$$\frac{d^2\mathbf{r}}{dt^2} + 2\boldsymbol{\omega} \times \frac{d\mathbf{r}}{dt} + \nabla U(\mathbf{r}) = \mathbf{a}_S + \mathbf{a}_{SEP}, \quad (1)$$

where $\boldsymbol{\omega} = \omega \hat{\mathbf{z}}$ ($\hat{\mathbf{z}}$ is a unit vector pointing in the direction \mathbf{z}) is the angular velocity vector of the rotating frame and \mathbf{r} is the position vector of the hybrid sail relative to the center of mass of the two primaries. Again, the small annual changes in the inclination of the Sun-line with respect to the plane of the system will not be considered. The three-body pseudo-potential $U(\mathbf{r})$, the solar radiation pressure acceleration \mathbf{a}_S and the nondimensional acceleration due to the SEP thruster

\mathbf{a}_{SEP} are defined by

$$U(\mathbf{r}) = -\left[\frac{1}{2}|\boldsymbol{\omega} \times \mathbf{r}|^2 + \frac{1-\mu}{r_1} + \frac{\mu}{r_2}\right],$$

$$\mathbf{a}_S = a_0(\mathbf{S} \cdot \mathbf{n})^2 \mathbf{n}, \quad (2)$$

$$\mathbf{a}_{SEP} = a_{SEP} \mathbf{m}, \quad (3)$$

where μ is the mass ratio for the Earth-Moon system. The hybrid sail position vectors w.r.t. m_1 and m_2 respectively (see Figure 1), are defined as $\mathbf{r}_1 = [x + \mu, y, z]^T$ and $\mathbf{r}_2 = [x - (1 - \mu), y, z]^T$, a_0 is the magnitude of the solar radiation pressure acceleration exerted on the hybrid sail and the unit vector \mathbf{n} denotes the thrust direction, \mathbf{a}_{SEP} is the acceleration from the SEP system and the unit vector \mathbf{m} denotes the thrust direction. The sail is oriented such that it is always directed along the Sun-line \mathbf{S} , pitched at an angle γ to provide a constant out-of-plane force. The unit normal to the hybrid sail surface \mathbf{n} and the Sun-line direction are given by

$$\mathbf{n} = [\cos(\gamma) \cos(\omega_* t) \quad -\cos(\gamma) \sin(\omega_* t) \quad \sin(\gamma)]^T, \quad (4)$$

$$\mathbf{S} = [\cos(\omega_* t) \quad -\sin(\omega_* t) \quad 0]^T, \quad (5)$$

where ω_* is the angular rate of the Sun-line in the corotating frame in a dimensionless synodic coordinate system.

Linearized System

The dynamics of the hybrid sail in the neighborhood of the libration points will now be investigated. The coordinates of the equilibrium point are defined as $\mathbf{r}_L = (x_{L_i}, y_{L_i}, z_{L_i})^T$ with $i = 1, \dots, 5$. Let a small displacement in \mathbf{r}_L be $\delta \mathbf{r}$ such that $\mathbf{r} \rightarrow \mathbf{r}_L + \delta \mathbf{r}$. The equations for the hybrid sail can then be written as

$$\frac{d^2 \delta \mathbf{r}}{dt^2} + 2\boldsymbol{\omega} \times \frac{d\delta \mathbf{r}}{dt} + \nabla U(\mathbf{r}_L + \delta \mathbf{r}) = \mathbf{a}_S(\mathbf{r}_L + \delta \mathbf{r}) + \mathbf{a}_{SEP}(\mathbf{r}_L + \delta \mathbf{r}), \quad (6)$$

and retaining only the first-order term in $\delta \mathbf{r} = (\xi, \eta, \zeta)^T$ in a Taylor-series expansion, the gradient of the potential and the acceleration can be expressed as

$$\nabla U(\mathbf{r}_L + \delta \mathbf{r}) = \nabla U(\mathbf{r}_L) + \left. \frac{\partial \nabla U(\mathbf{r})}{\partial \mathbf{r}} \right|_{\mathbf{r}=\mathbf{r}_L} \delta \mathbf{r} + O(\delta \mathbf{r}^2), \quad (7)$$

$$\mathbf{a}_S(\mathbf{r}_L + \delta \mathbf{r}) = \mathbf{a}_S(\mathbf{r}_L) + \left. \frac{\partial \mathbf{a}_S(\mathbf{r})}{\partial \mathbf{r}} \right|_{\mathbf{r}=\mathbf{r}_L} \delta \mathbf{r} + O(\delta \mathbf{r}^2). \quad (8)$$

$$\mathbf{a}_{SEP}(\mathbf{r}_L + \delta \mathbf{r}) = \mathbf{a}_{SEP}(\mathbf{r}_L) + \left. \frac{\partial \mathbf{a}_{SEP}(\mathbf{r})}{\partial \mathbf{r}} \right|_{\mathbf{r}=\mathbf{r}_L} \delta \mathbf{r} + O(\delta \mathbf{r}^2). \quad (9)$$

It is assumed that $\nabla U(\mathbf{r}_L) = 0$, and the accelerations \mathbf{a}_S and \mathbf{a}_{SEP} are constant with respect to the small displacement $\delta \mathbf{r}$, so that

$$\left. \frac{\partial \mathbf{a}_S(\mathbf{r})}{\partial \mathbf{r}} \right|_{\mathbf{r}=\mathbf{r}_L} = 0, \quad (10)$$

$$\left. \frac{\partial \mathbf{a}_{SEP}(\mathbf{r})}{\partial \mathbf{r}} \right|_{\mathbf{r}=\mathbf{r}_L} = 0. \quad (11)$$

The linear variational system associated with the libration points at \mathbf{r}_L can be determined through a Taylor series expansion by substituting Eqs. (7) and (8) into (6) so that

$$\frac{d^2\delta\mathbf{r}}{dt^2} + 2\boldsymbol{\omega} \times \frac{d\delta\mathbf{r}}{dt} - K\delta\mathbf{r} = \mathbf{a}_S(\mathbf{r}_L) + \mathbf{a}_{SEP}(\mathbf{r}_L), \quad (12)$$

where the matrix K is defined as

$$K = - \left[\frac{\partial \nabla U(\mathbf{r})}{\partial \mathbf{r}} \Big|_{\mathbf{r}=\mathbf{r}_L} \right]. \quad (13)$$

Using matrix notation the linearised equation about the libration point (Equation (12)) can be represented by the inhomogeneous linear system $\dot{\mathbf{X}} = A\mathbf{X} + \mathbf{b}(t)$, where the state vector $\mathbf{X} = (\delta\mathbf{r}, \delta\dot{\mathbf{r}})^T$, and for which $\mathbf{b}(t)$ (a 6×1 vector) is equal to the sum of control accelerations of the sail and the SEP.

The Jacobian matrix A has the general form

$$A = \begin{pmatrix} 0_3 & I_3 \\ K & \Omega \end{pmatrix}, \quad (14)$$

where I_3 is a identity matrix, and

$$\Omega = \begin{pmatrix} 0 & 2 & 0 \\ -2 & 0 & 0 \\ 0 & 0 & 0 \end{pmatrix}. \quad (15)$$

Again, the sail attitude is fixed such that the sail normal vector \mathbf{n} , which is the unit vector that is perpendicular to the sail surface, points always along the direction of the Sun-line with the following constraint $\mathbf{S} \cdot \mathbf{n} \geq 0$. Its direction is described by the pitch angle γ relative to the Sun-line, which represents the sail attitude. By making the transformation $\mathbf{r} \rightarrow \mathbf{r}_L + \delta\mathbf{r}$ and retaining only the first-order term in $\delta\mathbf{r} = (\xi, \eta, \zeta)^T$ in the Taylor-series expansion where (ξ, η, ζ) are axes attached to the libration point as shown in Figure 1 (a), the linearized nondimensional equations of motion relative to the collinear libration points can be written as

$$\ddot{\xi} - 2\dot{\eta} - U_{xx}^o \xi = a_\xi + a_{SEP_\xi}, \quad (16)$$

$$\ddot{\eta} + 2\dot{\xi} - U_{yy}^o \eta = a_\eta + a_{SEP_\eta}, \quad (17)$$

$$\ddot{\zeta} - U_{zz}^o \zeta = a_\zeta + a_{SEP_\zeta}, \quad (18)$$

where U_{xx}^o , U_{yy}^o , and U_{zz}^o are the partial derivatives of the gravitational potential evaluated at the collinear libration points, and the solar sail acceleration is defined in terms of three auxiliary variables a_ξ , a_η , and a_ζ . The solar sail acceleration components are again given by

$$a_\xi = a_0 \cos(\omega_\star t) \cos^3(\gamma), \quad (19)$$

$$a_\eta = -a_0 \sin(\omega_\star t) \cos^3(\gamma), \quad (20)$$

$$a_\zeta = a_0 \cos^2(\gamma) \sin(\gamma), \quad (21)$$

where a_0 is the characteristic acceleration. The SEP acceleration components \mathbf{a}_{SEP} are used for feedback control as described later.

TRACKING BY FEEDBACK LINEARIZATION

From equation (1) the motion of the hybrid solar sail in the CRTBP is described by the scalar equations in the form

$$\ddot{\xi} = 2\dot{\eta} + (x_{L_2} + \xi) - (1 - \mu) \frac{(x_{L_2} + \xi) + \mu}{r_1^3} - \mu \frac{(x_{L_2} + \xi) - 1 + \mu}{r_2^3} + a_\xi + u_\xi, \quad (22)$$

$$\ddot{\eta} = -2\dot{\xi} + \eta - \left(\frac{1 - \mu}{r_1^3} + \frac{\mu}{r_2^3} \right) \eta + a_\eta + u_\eta, \quad (23)$$

$$\ddot{\zeta} = - \left(\frac{1 - \mu}{r_1^3} + \frac{\mu}{r_2^3} \right) \zeta + a_\zeta + u_\zeta, \quad (24)$$

where the vector

$$\mathbf{u}(t) = [u_\xi \quad u_\eta \quad u_\zeta]^T \quad (25)$$

is the applied control acceleration due to the SEP thruster, such that $\mathbf{u}(t) \triangleq \mathbf{a}_{SEP}$.

To develop a feedback linearization scheme, the motion of the hybrid solar sail moving in the CRTBP is separated into linear and nonlinear components, such that

$$\ddot{\xi} = f_{Non-Linear}^\xi + f_{Linear}^\xi + a_\xi + u_\xi, \quad (26)$$

$$\ddot{\eta} = f_{Non-Linear}^\eta + f_{Linear}^\eta + a_\eta + u_\eta, \quad (27)$$

$$\ddot{\zeta} = f_{Non-Linear}^\zeta + f_{Linear}^\zeta + a_\zeta + u_\zeta, \quad (28)$$

where the f functions are defined as the linear and the nonlinear terms in the equations (22), (23) and (24)

$$f_{Non-Linear}^\xi = -(1 - \mu) \frac{(x_{L_2} + \xi) + \mu}{r_1^3} - \mu \frac{(x_{L_2} + \xi) - 1 + \mu}{r_2^3}, \quad (29)$$

$$f_{Linear}^\xi = 2\dot{\eta} + (x_{L_2} + \xi), \quad (30)$$

$$f_{Non-Linear}^\eta = - \left(\frac{1 - \mu}{r_1^3} + \frac{\mu}{r_2^3} \right) \eta, \quad (31)$$

$$f_{Linear}^\eta = -2\dot{\xi} + \eta, \quad (32)$$

$$f_{Non-Linear}^\zeta = - \left(\frac{1 - \mu}{r_1^3} + \frac{\mu}{r_2^3} \right) \zeta, \quad (33)$$

$$f_{Linear}^\zeta = 0, \quad (34)$$

with $r_1 = \sqrt{((x_{L_2} + \xi) + \mu)^2 + \eta^2 + \zeta^2}$ and $r_2 = \sqrt{((x_{L_2} + \xi) - 1 + \mu)^2 + \eta^2 + \zeta^2}$.

The solar sail acceleration components are given in equations (19), (20) and (21). The SEP control $\mathbf{u}(t)$ is then selected such that

$$\mathbf{u}(t) = \begin{bmatrix} u_\xi \\ u_\eta \\ u_\zeta \end{bmatrix} = \mathbf{U}(t) + \tilde{\mathbf{u}}(t), \quad (35)$$

where

$$\mathbf{U}(t) = - \begin{bmatrix} (x_{L_2} + \xi) - (1 - \mu) \frac{(x_{L_2} + \xi) + \mu}{r_1^3} - \mu \frac{(x_{L_2} + \xi) - 1 + \mu}{r_2^3} - U_{xx}^o \xi \\ - \left(\frac{1 - \mu}{r_1^3} + \frac{\mu}{r_2^3} \right) \eta - U_{yy}^o \eta \\ - \left(\frac{1 - \mu}{r_1^3} + \frac{\mu}{r_2^3} \right) \zeta - U_{zz}^o \zeta \end{bmatrix} \quad (36)$$

is the canceling term and $\tilde{\mathbf{u}}(t)$ the stabilising term.

The equations (22), (23) and (24) then become

$$\ddot{\xi} = 2\dot{\eta} + U_{xx}^o \xi + a_0 \cos(\omega_* t) \cos^3(\gamma) + \tilde{u}_\xi, \quad (37)$$

$$\ddot{\eta} = -2\dot{\xi} + U_{yy}^o \eta - a_0 \sin(\omega_* t) \cos^3(\gamma) + \tilde{u}_\eta, \quad (38)$$

$$\ddot{\zeta} = U_{zz}^o \zeta + a_0 \cos^2(\gamma) \sin(\gamma) + \tilde{u}_\zeta. \quad (39)$$

By removing the nonlinear dynamics from the system, the control acceleration vector $\tilde{\mathbf{u}}(t)$ is determined such that the desired response characteristics of the linear time-invariant dynamics are produced and so Eq. (37) - (39) are identical to the linear system defined by Eq. (16) - (18). In particular, it can be ensured that the displacement distance of the periodic orbit is constant, which provides key advantages for lunar polar telecommunications.

TRACKING A REFERENCE TRAJECTORY

After transforming the nonlinear dynamics into a linear form, one can easily design controllers for either stabilization or tracking purposes.

Linear Feedback Control

Let us consider the nonlinear system described by

$$\ddot{\mathbf{x}} = f(\mathbf{x}, \dot{\mathbf{x}}) + \mathbf{u}, \quad (40)$$

where $\mathbf{x} \in \mathbb{R}^3$ is the position. Let $\mathbf{e}(t) = \mathbf{x}(t) - \mathbf{x}_{ref}(t)$ denote the position error relative to some reference solution, where the reference trajectory

$$\mathbf{x}_{ref}(t) = [\xi_{ref} \quad \eta_{ref} \quad \zeta_{ref}]^T \quad (41)$$

is given by the analytical solution

$$\xi_{ref}(t) = \xi_0 \cos(\omega_* t), \quad (42)$$

$$\eta_{ref}(t) = \eta_0 \sin(\omega_* t), \quad (43)$$

$$\zeta_{ref}(t) = \zeta_0. \quad (44)$$

The term $\mathbf{e}(t)$ is then differentiated until the control appears so that

$$\mathbf{e}(t) = \mathbf{x}(t) - \mathbf{x}_{ref}(t), \quad (45)$$

$$\dot{\mathbf{e}}(t) = \dot{\mathbf{x}}(t) - \dot{\mathbf{x}}_{ref}(t), \quad (46)$$

$$\begin{aligned} \ddot{\mathbf{e}}(t) &= \ddot{\mathbf{x}}(t) - \ddot{\mathbf{x}}_{ref}(t), \\ &= f(\mathbf{x}, \dot{\mathbf{x}}) + \mathbf{u} - \ddot{\mathbf{x}}_{ref}(t), \\ &= -\lambda_1 \dot{\mathbf{e}} - \lambda_2 \mathbf{e}, \end{aligned} \quad (47)$$

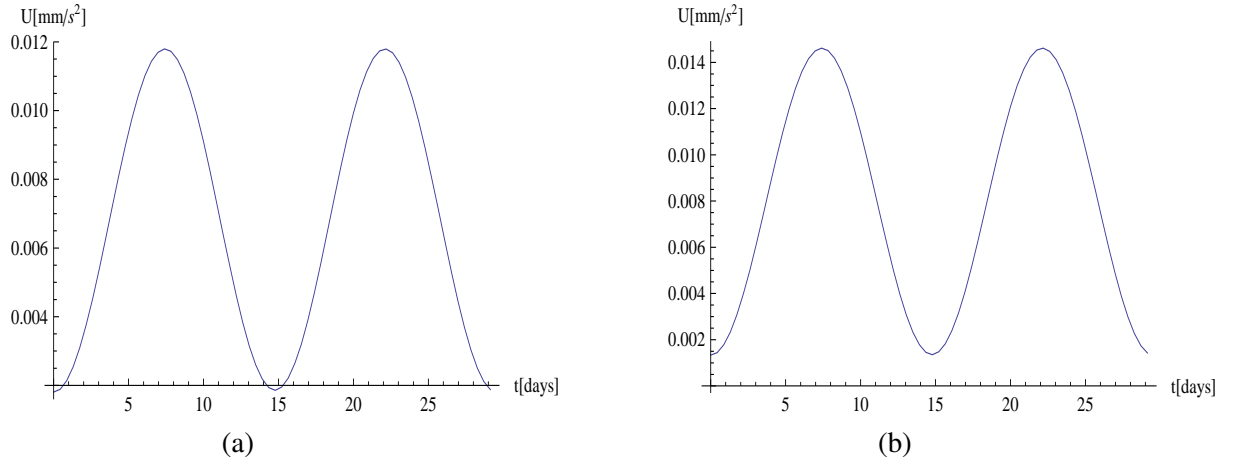


Figure 3 (a) Magnitude of the total control effort about the L_1 point; (b) Magnitude of the total control effort about the L_2 point.

and so

$$\mathbf{u}(t) = -f(\mathbf{x}, \dot{\mathbf{x}}) + \ddot{\mathbf{x}}_{ref}(t) - \lambda_1 \dot{\mathbf{e}} - \lambda_2 \mathbf{e}, \quad (48)$$

where

$$f = \begin{bmatrix} f_{Non-Linear}^{\xi} \\ f_{Non-Linear}^{\eta} \\ f_{Non-Linear}^{\zeta} \end{bmatrix} \quad (49)$$

and $-\lambda_1 \dot{\mathbf{e}} - \lambda_2 \mathbf{e}$ is the stabilizing term.

Trajectory Tracking

Consider the system given by equation (40), where our objective is to make the output $\mathbf{x} \in \mathbb{R}^3$ track a desired trajectory given by the reference trajectory $\mathbf{x}_{ref} \in \mathbb{R}^3$ while keeping the position bounded. Therefore, a control law for the input $\tilde{\mathbf{u}} \in \mathbb{R}^3$ will be found, such that starting from any initial position in a domain $D \subset \mathbb{R}^3$, the tracking error $\mathbf{e}(t) = \mathbf{x}(t) - \mathbf{x}_{ref}(t)$ goes to zero. Hence, asymptotic tracking will be achieved if a state feedback control law is designed to ensure that $\mathbf{e}(t)$ is bounded and converges to zero as t tends to infinity. Thus, the control law

$$\tilde{\mathbf{u}} = -\lambda_1 \dot{\mathbf{e}} - \lambda_2 \mathbf{e} \quad (50)$$

yields the tracking error equation

$$\ddot{\mathbf{e}} + \lambda_1 \dot{\mathbf{e}} + \lambda_2 \mathbf{e} = 0, \quad (51)$$

where λ_1 and λ_2 are chosen positive constants.

EVALUATION OF HYBRID SAIL PERFORMANCE

Evaluation

Let us investigate the performance of a hybrid sail system, constituted by a solar sail combined with solar electric propulsion. A minimum displacement distance of 1750 km has been considered

Table 1. Parameters of reference trajectory.

	$\xi_0[km]$	$\eta_0[km]$	$\zeta_0[km]$	$a_0[mm/s^2]$
L_1	-422.849	-4108.13	1750	0.16
L_2	282.613	-5525.23	1750	0.10

for the simulations, as given in Table 1. This allows the spacecraft to view both the lunar pole and the Earth for communication applications. The simulation was performed around the collinear libration points for a period of one month. The magnitude of the total control effort appears in Figure 3. Thus, the control acceleration effort $U(t)$ required to track the reference orbit while rejecting the nonlinearities varies up to 0.004 (0.012 mm/s^2) for the orbit about L_1 and 0.005 (0.014 mm/s^2) for the orbit about the L_2 point. The control accelerations are continuous smooth signals. The acceleration derived from the solar sail (denoted by a_ξ, a_η, a_ζ) is plotted in terms of components for one-month orbits in Figure 4 (a) about L_1 , Figure 6 (a) about L_2 , and the SEP acceleration components appears in Figure 4 (b) about L_1 , Figure 6 (b) about L_2 . The control acceleration effort derived from the thruster (denoted by U_ξ, U_η, U_ζ) is order of $10^{-3} - 10^{-4}$, while the acceleration derived from the solar sail is approximately 10^{-2} . The small control acceleration from the SEP thruster is then applied to ensure that the displacement of the periodic orbit is constant. The solar sail provides a constant out-of-plane force. Figure 5 (critically damped motion) illustrates the position error components with $e(0) = (-42.28, -410.81, 175)^T \text{ km}$, denoted by e_ξ, e_η, e_ζ and the velocity error components, denoted by $e_{\xi d}, e_{\eta d}, e_{\zeta d}$, under the nonlinear control and the SEP thruster around L_1 . Figure 7 (critically damped motion) shows the corresponding errors in the position with $e(0) = (28.26, -552.52, 175)^T \text{ km}$ and velocity components around L_2 .

These figures show that the motion is bounded and periodic. This observation implies that the augmented thrust acceleration ensures a constant displacement orbit. The orbit resulting from tracking the reference orbit using the nonlinear control and the SEP thruster around L_1 are also depicted in Figure 8 (a) and Figure 8 (b) for the orbit around L_2 point.

The parameters of the reference trajectory used for the simulations are summarised in Table 1.

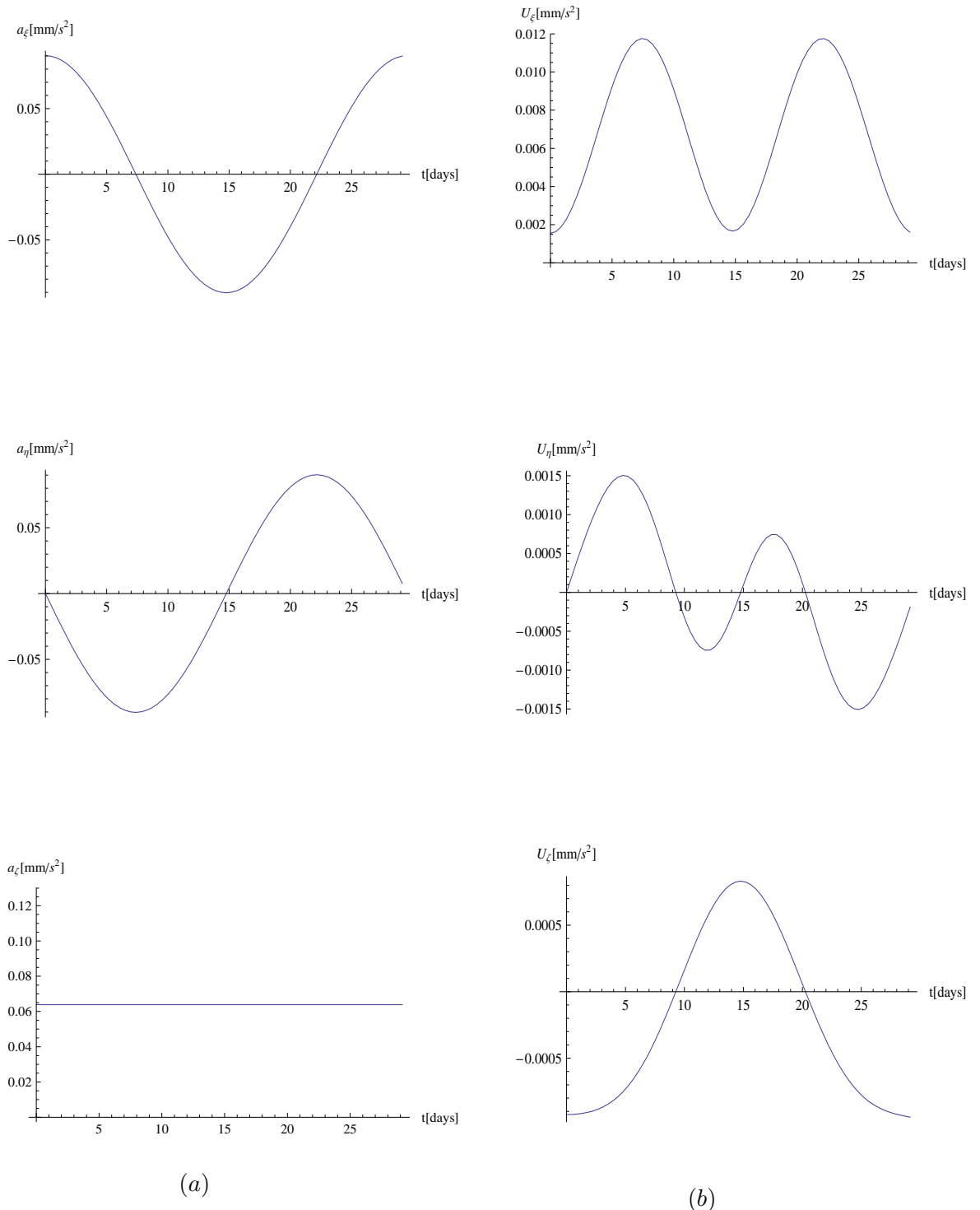
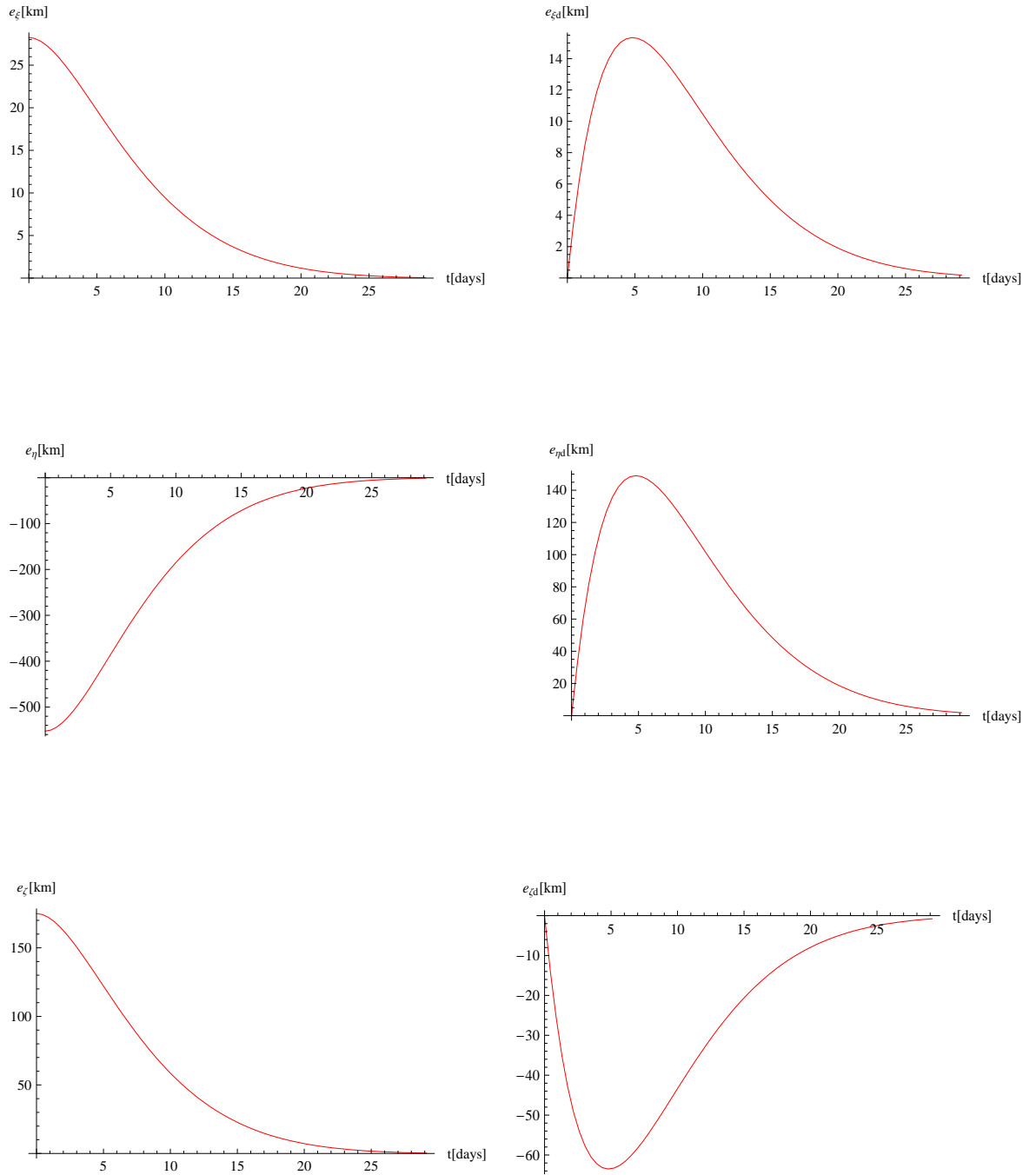


Figure 4 (a) Acceleration derived from the solar sail about the L_1 point; (b) Acceleration derived from the thruster about the L_1 point.



(a)

(b)

Figure 5 (a) Position error components about the L_1 point; (b) Velocity Error components about the L_1 point.

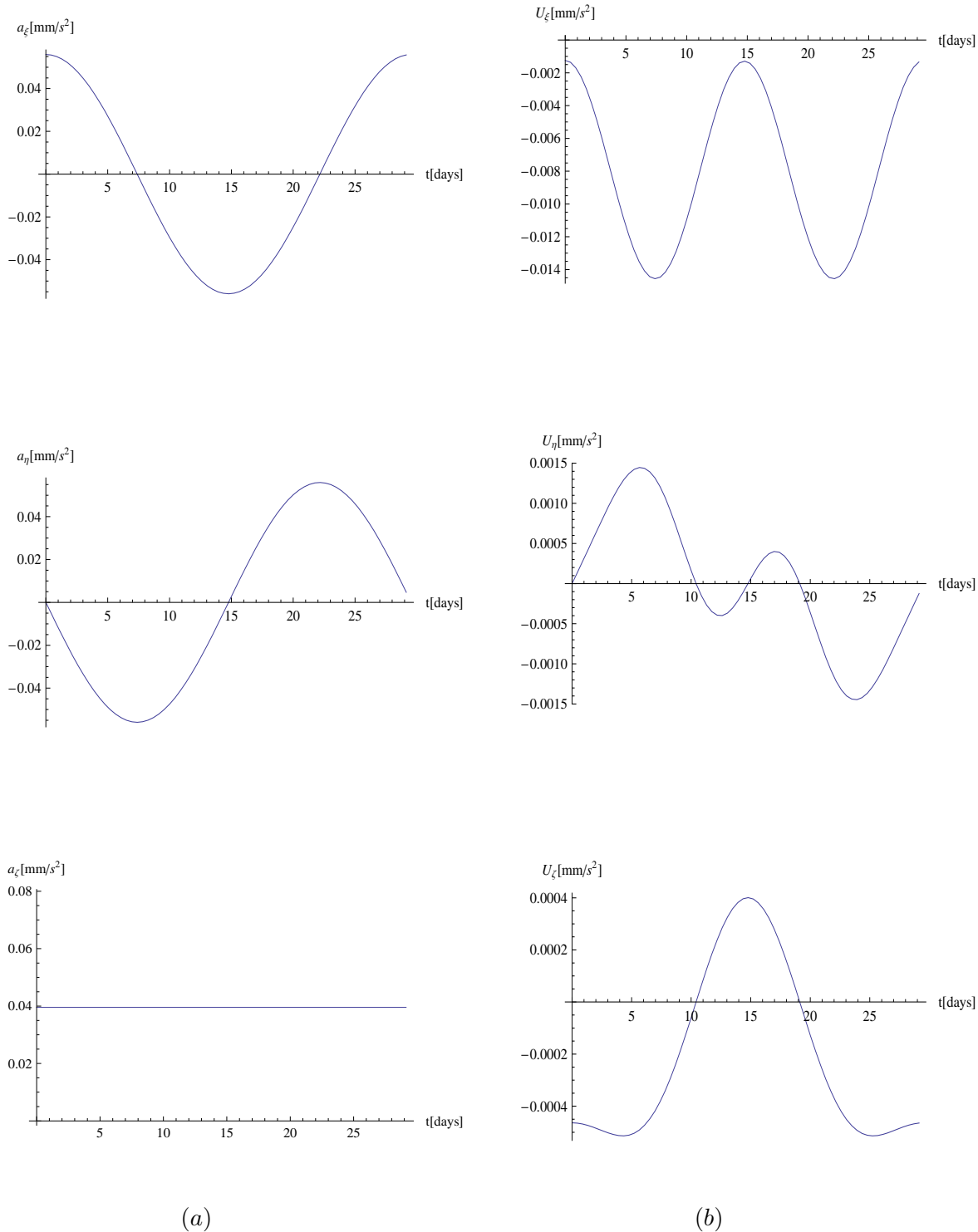


Figure 6 (a) Acceleration derived from the solar sail about the L_2 point; (b) Acceleration derived from the SEP thruster about the L_2 point.

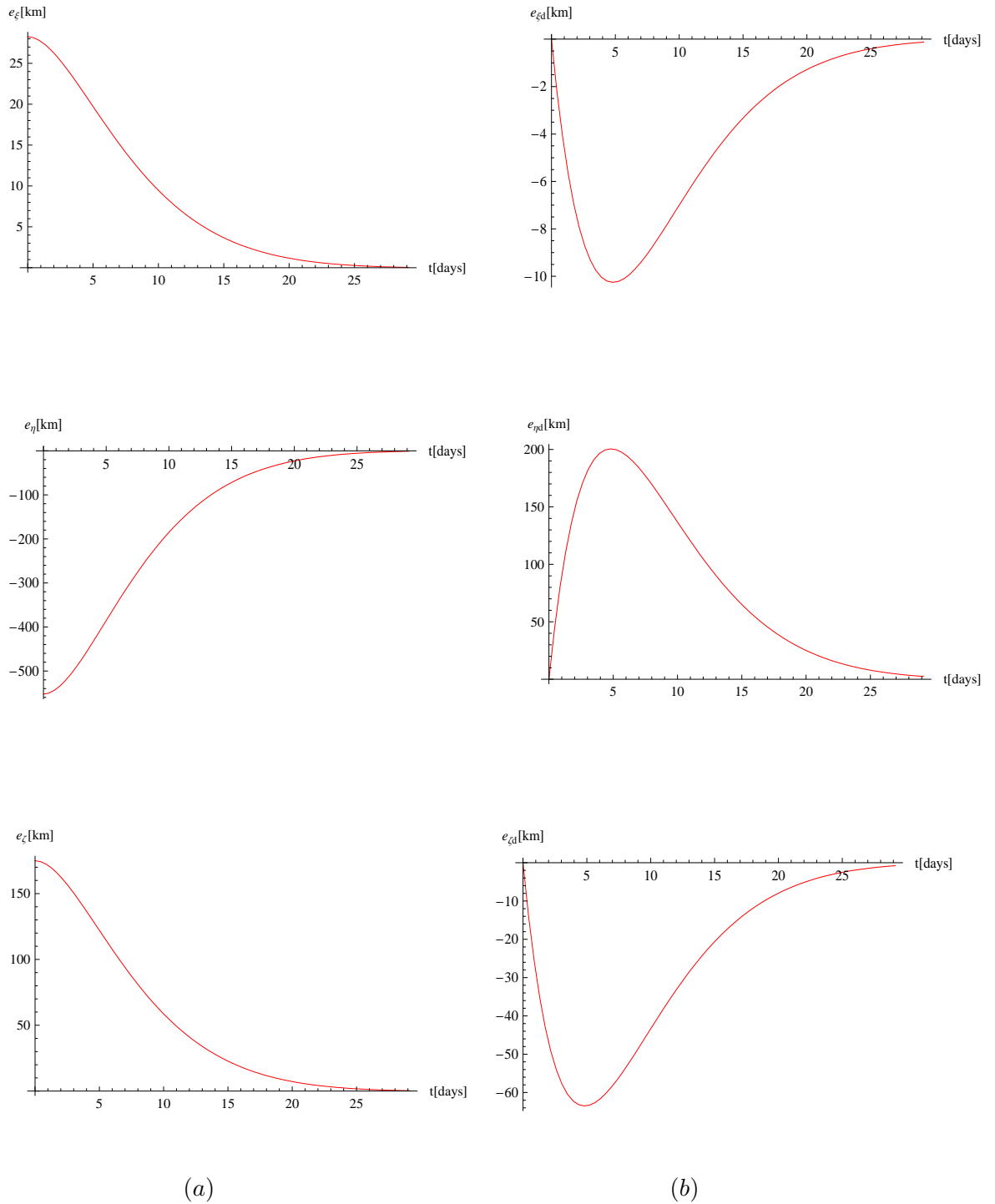
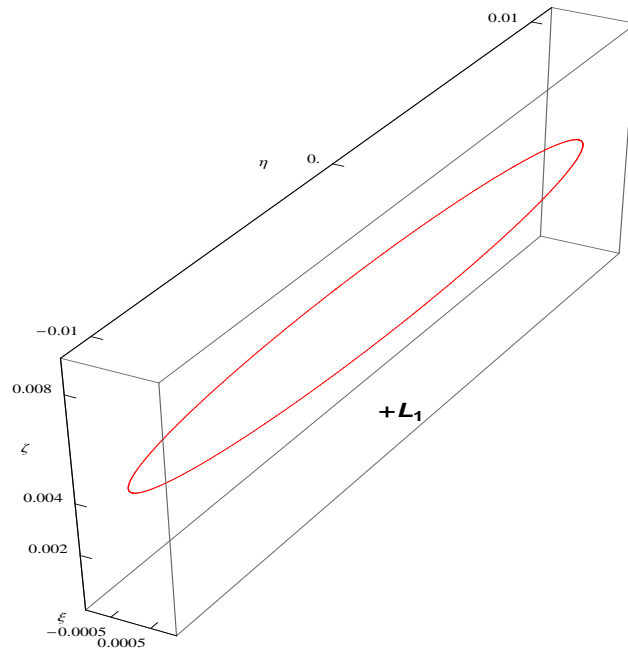
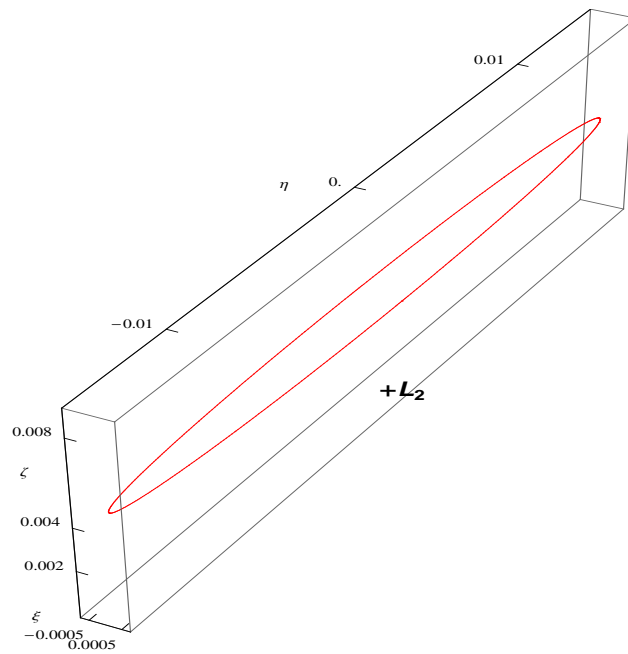


Figure 7 (a) Position error components about the L_2 point; (b) Velocity Error components about the L_2 point.



(a)



(b)

Figure 8 Orbit resulting from tracking the reference orbit using the nonlinear control and SEP thruster: (a) Above L_1 ; (b) Above L_2 .

Propellant Usage

Propellant usage for the SEP thruster is proportional to the total ΔV , which is the integration over time of the magnitude of the control acceleration produced by using the SEP thruster so that

$$\Delta V = \int_0^{2\pi/\omega_*} |\mathbf{u}| dt. \quad (52)$$

The total ΔV_{Total} over a 5 year mission is given by

$$\Delta V_{Total} = \Delta V_{per\ orbit} \times no, \quad (53)$$

where no is the total number of orbits. Once the total ΔV is computed, the propellant usage can be found using the rocket equation.

Let us define the mass m of the rocket at a time t , as a function of the initial mass m_i , ΔV and the effective exhaust velocity $v_e = I_{sp} \cdot g$,

$$m = m_i e^{-\Delta V/g \cdot I_{sp}}. \quad (54)$$

The mass of propellant is then the difference between the initial and the final masses

$$m_{prop} = m_i - m = m_i(1 - e^{-\Delta V_{Total}/g \cdot I_{sp}}), \quad (55)$$

where I_{sp} is the specific impulse ($\approx 3000\ sec$ for an electric thruster).

Assume a specific impulse of $I_{sp} = 3000\ sec$ and an initial mass of $m_i = 500\ kg$, it is obtained from equation (52) the average ΔV per orbit of approximately $23\ m/s$. Then, the total ΔV per orbit over 5 years is $1536\ m/s$. The consumed propellant mass is then $m_{prop} = 25\ kg$. The parameters are summarized in Table 2.

Table 2. Summary of Parameters.

<i>Parameter</i>	<i>Description</i>	<i>Value</i>
m_i (kg)	Initial Mass	500
I_{sp} (sec)	Specific Impulse	3000
ΔV_{Total} (m/s)	Total ΔV over 5 years	1536
m_{prop} (kg)	Propellant Mass Consumed (kg)	25

IMPULSE CONTROL

The displaced orbits investigated in the previous sections may also be generated using impulse control. The out-of-plane displacement is then achieved by repeatedly reversing the vertical component of the spacecraft velocity in a periodic manner. In order to compare the continuous thrust and impulse control orbits, linearized equations of motion will now be considered for small displacements, as shown in Figure 9. The representation of this technique can be seen in Figure 10. The nondimensional linearized equations of motion near the collinear libration points are given by

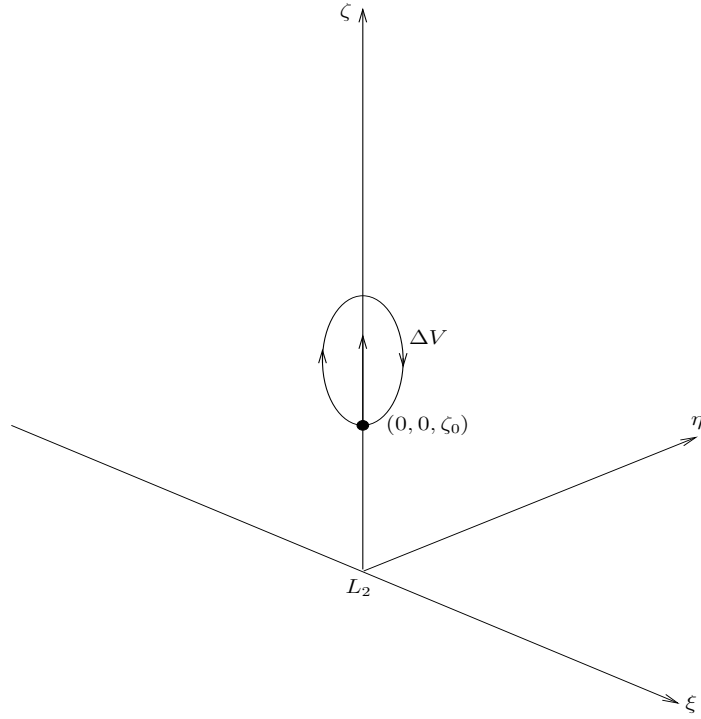


Figure 9. Orbit reference frame for impulse control (Out-of-plane maneuvers).

$$\ddot{\xi} - 2\dot{\eta} - U_{xx}^o \xi = a_{\xi}, \quad (56)$$

$$\ddot{\eta} + 2\dot{\xi} - U_{yy}^o \eta = a_{\eta}, \quad (57)$$

$$\ddot{\zeta} - U_{zz}^o \zeta = a_{\zeta}, \quad (58)$$

where U_{xx}^o , U_{yy}^o , and U_{zz}^o are the partial derivatives of the gravitational potential evaluated at the collinear libration points.

For continuous thrust, the required acceleration components for displaced artificial equilibrium solutions may be obtained from Eqs. ((56)-(58)) as

$$a_{\xi} = -U_{xx}^o \xi,$$

$$a_{\eta} = -U_{yy}^o \eta,$$

$$a_{\zeta} = -U_{zz}^o \zeta.$$

Out-of-plane Maneuvers

In order to maintain an out-of-plane displacement, repeated vertical impulses are required such that $\zeta(0) = \zeta(T) = \zeta_0$, where T is the period between impulses. It is found that

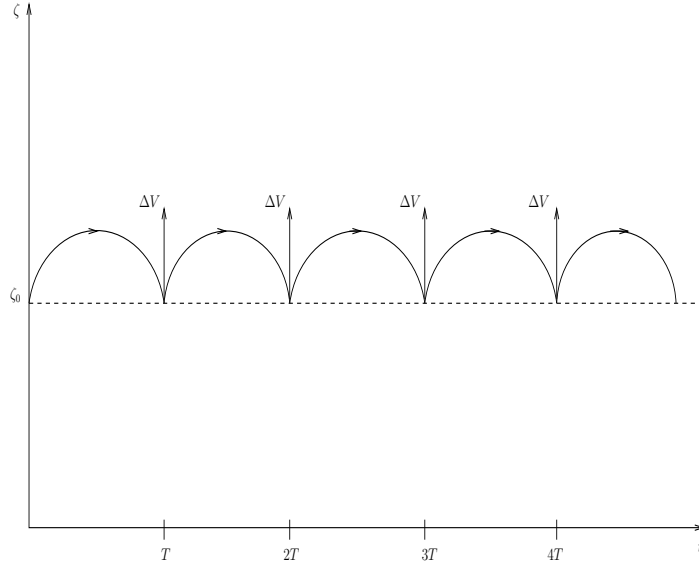


Figure 10. Impulse control scheme.

$$\cos(\omega_\zeta T) + \frac{\dot{\zeta}_0}{\omega_\zeta \zeta_0} \sin(\omega_\zeta T) = 1, \quad (59)$$

$$\frac{\dot{\zeta}_0}{\omega_\zeta \zeta_0} = \frac{1 - \cos(\omega_\zeta T)}{\sin(\omega_\zeta T)}, \quad (60)$$

$$\dot{\zeta}_0 = \omega_\zeta \zeta_0 \left[\frac{1 - \cos(\omega_\zeta T)}{\sin(\omega_\zeta T)} \right]. \quad (61)$$

Thus, the required initial out-of-plane velocity reduces to

$$\dot{\zeta}_0 = \omega_\zeta \zeta_0 \tan \left[\frac{\omega_\zeta T}{2} \right]. \quad (62)$$

There is an important symmetry in these equations of motion given by $\dot{\zeta}(T) = -\dot{\zeta}(0)$. This symmetry can thus be exploited, in a standard way, to obtain the effective out-of-plane acceleration \bar{a}_ζ by the repeated impulses. More explicitly

$$\bar{a}_\zeta \approx \frac{\Delta V_\zeta}{T} = \frac{2\dot{\zeta}_0}{T}, \quad (63)$$

and

$$\bar{a}_\zeta = \frac{2\omega_\zeta \zeta_0}{T} \tan \left[\frac{\omega_\zeta T}{2} \right]. \quad (64)$$

Let us assume now that the time between impulses is small. In this case, the effective out-of-plane acceleration can be approximated as

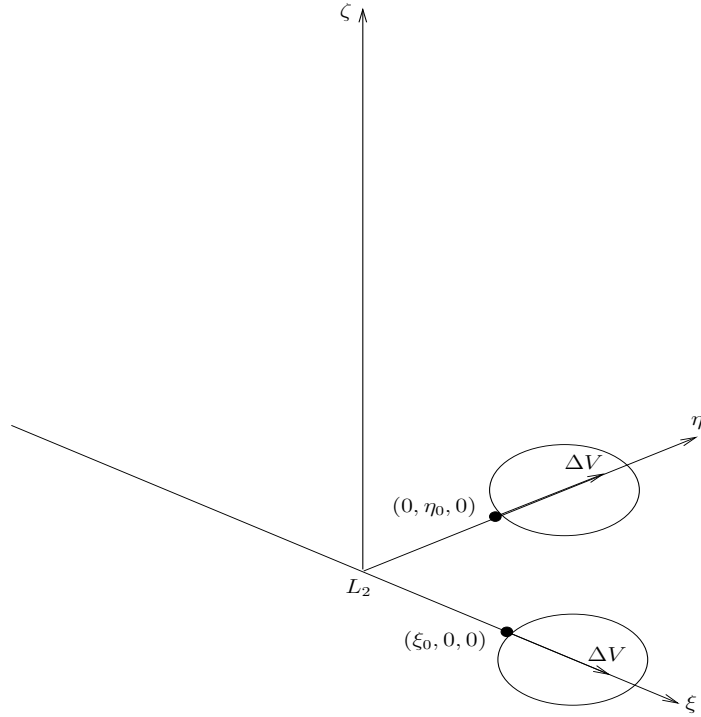


Figure 11. Orbit reference frame for impulse control (in-plane maneuvers).

$$\bar{a}_\zeta \approx \omega_\zeta^2 \zeta_0 + \frac{1}{12} \omega_\zeta^4 \zeta_0 T^2 + \dots \quad (65)$$

The relative displacement is given by

$$\begin{aligned} \Delta\zeta &= \zeta_{max} - \zeta_0, \\ &= \zeta\left(\frac{T}{2}\right) - \zeta_0, \\ &= -\zeta_0 \left[1 - \cos\left(\frac{\omega_\zeta T}{2}\right) \right] + \frac{\dot{\zeta}_0}{\omega_\zeta} \sin\left(\frac{\omega_\zeta T}{2}\right), \\ &= -2\zeta_0 \sin^2\left(\frac{\omega_\zeta T}{4}\right) + \frac{\dot{\zeta}_0}{\omega_\zeta} \sin\left(\frac{\omega_\zeta T}{2}\right). \end{aligned} \quad (66)$$

By the use of equation (62), equation (66) can be rewritten as

$$\Delta\zeta = \xi_0 \left[-2 \sin^2\left(\frac{\omega_\zeta T}{4}\right) + \sin\left(\frac{\omega_\zeta T}{2}\right) \tan\left(\frac{\omega_\zeta T}{2}\right) \right]. \quad (67)$$

In-plane Maneuvers

Assume that a radial displacement has been performed, then the following conditions will be used

$$\xi(0) = \xi(T) = \xi_0, \quad (68)$$

$$\eta(0) = \eta(T) = \eta_0. \quad (69)$$

The representation of this technique is given in Figure 11. It is obtained for the in-plane motion, respectively

$$\xi(0) = A_3 + A_4 = \xi_0, \quad (70)$$

$$\xi(T) = A_3 e^{\lambda_3 T} + A_4 e^{\lambda_4 T} = \xi_0, \quad (71)$$

and

$$\eta(0) = B_3 + B_4 = \eta_0, \quad (72)$$

$$\eta(T) = B_3 e^{\lambda_3 T} + B_4 e^{\lambda_4 T} = \eta_0. \quad (73)$$

In matrix form the system of equations above can be written as

$$\begin{bmatrix} 1 & 1 \\ e^{\lambda_3 T} & e^{\lambda_4 T} \end{bmatrix} \begin{bmatrix} A_3 \\ A_4 \end{bmatrix} = \begin{bmatrix} \xi_0 \\ \xi_0 \end{bmatrix}, \quad (74)$$

and

$$\begin{bmatrix} 1 & 1 \\ e^{\lambda_3 T} & e^{\lambda_4 T} \end{bmatrix} \begin{bmatrix} B_3 \\ B_4 \end{bmatrix} = \begin{bmatrix} \eta_0 \\ \eta_0 \end{bmatrix}. \quad (75)$$

Solving equation (74) (resp. equation (75)) for A_3 and A_4 (resp. for B_3 and B_4), yields the coefficients A_3 , A_4 , B_3 and B_4

$$\begin{bmatrix} A_3 \\ A_4 \end{bmatrix} = \frac{1}{-e^{\lambda_3 T} + e^{\lambda_4 T}} \begin{bmatrix} e^{\lambda_4 T} & -1 \\ -e^{\lambda_3 T} & 1 \end{bmatrix} \begin{bmatrix} \xi_0 \\ \xi_0 \end{bmatrix}, \quad (76)$$

$$\begin{bmatrix} B_3 \\ B_4 \end{bmatrix} = \frac{1}{-e^{\lambda_3 T} + e^{\lambda_4 T}} \begin{bmatrix} e^{\lambda_4 T} & -1 \\ -e^{\lambda_3 T} & 1 \end{bmatrix} \begin{bmatrix} \eta_0 \\ \eta_0 \end{bmatrix}, \quad (77)$$

and

$$A_3 = \frac{\xi_0}{-e^{\lambda_3 T} + e^{\lambda_4 T}} \left(e^{\lambda_4 T} - 1 \right), \quad (78)$$

$$A_4 = \frac{\xi_0}{-e^{\lambda_3 T} + e^{\lambda_4 T}} \left(-e^{\lambda_3 T} + 1 \right), \quad (79)$$

Table 3. Requirements for displaced lunar orbits.

<i>Altitude(km)</i>	1750	2000	2500
a_0 ($mm s^{-2}$)	0.1	0.11	0.14
$\Delta V a$ (ms^{-1})	23	26	32
$\Delta V b$ (ms^{-1})	24.19	27.64	34.56

a Accumulated ΔV for low-thrust propulsion.

b Accumulated ΔV per orbit for impulse control (4 impulses per orbit).

$$B_3 = \frac{\eta_0}{-e^{\lambda_3 T} + e^{\lambda_4 T}} \left(e^{\lambda_4 T} - 1 \right), \quad (80)$$

$$B_4 = \frac{\eta_0}{-e^{\lambda_3 T} + e^{\lambda_4 T}} \left(-e^{\lambda_3 T} + 1 \right). \quad (81)$$

Thus, the required initial velocity components are given respectively by

$$\begin{aligned} \dot{\xi}(0) &= \lambda_3 A_3 + \lambda_4 A_4, \\ &= \frac{\xi_0}{-e^{\lambda_3 T} + e^{\lambda_4 T}} \left[\lambda_3 (e^{\lambda_4 T} - 1) + \lambda_4 (-e^{\lambda_3 T} + 1) \right], \end{aligned} \quad (82)$$

$$\begin{aligned} \dot{\eta}(0) &= \lambda_3 B_3 + \lambda_4 B_4, \\ &= \frac{\eta_0}{-e^{\lambda_3 T} + e^{\lambda_4 T}} \left[\lambda_3 (e^{\lambda_4 T} - 1) + \lambda_4 (-e^{\lambda_3 T} + 1) \right]. \end{aligned} \quad (83)$$

If at time $t = 0$, the relative position ξ_0 , η_0 and ζ_0 is known, then the relative velocity components $\dot{\xi}(0)$, $\dot{\eta}(0)$ and $\dot{\zeta}(0)$ can be determined. The components of the initial velocity are given by

$$\mathbf{V}(0) = \left[\dot{\xi}(0) \quad \dot{\eta}(0) \quad \dot{\zeta}(0) \right]^T. \quad (84)$$

The terms $\dot{\xi}(T)$, $\dot{\eta}(T)$ and $\dot{\zeta}(T)$ are then the velocity components at time $t = T$ imparted along the ξ , η and ζ respectively, and denoted by

$$\mathbf{V}(T) = \left[\dot{\xi}(T) \quad \dot{\eta}(T) \quad \dot{\zeta}(T) \right]^T. \quad (85)$$

Thus, the magnitude of the velocity impulse vector $\Delta \mathbf{V}$ in all directions is given by

$$\begin{aligned} |\Delta \mathbf{V}| &= |\mathbf{V}(T) - \mathbf{V}(0)|, \\ &= \sqrt{(\dot{\xi}(T) - \dot{\xi}(0))^2 + (\dot{\eta}(T) - \dot{\eta}(0))^2 + (\dot{\zeta}(T) - \dot{\zeta}(0))^2}. \end{aligned} \quad (86)$$

The requirements for impulse control and continuous thrust for different values of out-of-plane distance are shown in Table 3. For example a constant displacement distance of 1750 km requires an acceleration of 0.1 mm^{-2} , which correspond to a ΔV of 23 m.s^{-1} per orbit for the continuous thrust control. Similarly, for impulse control using 4 impulses per orbit, the required ΔV is 24.19 m.s^{-1} per orbit.

CONCLUSIONS

A hybrid concept for displaced periodic orbits in the Earth-Moon system has been developed. A feedback linearization was used to perform stabilization and trajectory tracking for nonlinear systems. The idea of this control is to transform a given nonlinear system into a linear system by use of a nonlinear coordinate transformation and nonlinear feedback. The augmented thrust acceleration is then applied to ensure a constant displacement periodic orbit, which provides key advantages for lunar polar telecommunications. A stabilizing approach is then introduced to increase the damping in the system and to allow a higher gain in the controller. Theoretical and simulation results show good performance, with modest propellant mass requirements ($m_{prop} = 25 \text{ kg}$). Impulse control has also been investigated as an alternative to continuous thrust control.

REFERENCES

- [1] C. R. McInnes, *Solar sailing: technology, dynamics and mission applications*. London: Springer Praxis, 1999.
- [2] T. Waters and C. McInnes, "Periodic Orbits Above the Ecliptic in the Solar-Sail Restricted Three-Body Problem," *J. of Guidance, Control, and Dynamics*, Vol. 30, No. 3, 2007, pp. 687–693.
- [3] J. Simo and C. R. McInnes, "Solar sail trajectories at the Earth-Moon Lagrange points," *In 59th International Astronautical Congress*, Glasgow, Scotland, 29 Sep - 03 Oct 2008. Paper IAC-08.C1.3.13.
- [4] J. Simo and C. R. McInnes, "Stabilization of Displaced Periodic Orbits in the Solar Sail Restricted Three-Body Problem," *presented at the SIAM Conference on Applications of Dynamical Systems (DS09)*, Snowbird, Utah, May 17 - 21, 2009.
- [5] J. Simo and C. R. McInnes, "Asymptotic Analysis of Displaced Lunar Orbits," *Journal of Guidance, Control and Dynamics*, Vol. 32, No. 5, September-October 2009, pp. 1666–1671.
- [6] J. Simo and C. R. McInnes, "Analysis and Control of Displaced Periodic Orbits in the Earth-Moon System," *In 60th International Astronautical Congress*, Daejeon, Republic of Korea, 12 - 16 October 2009. IAC-09.C1.2.4.
- [7] J. Simo and C. R. McInnes, "Displaced Periodic Orbits with Low-Thrust Propulsion in the Earth-Moon System," *In 19th AAS/AIAA Space Flight Mechanics Meeting*, Savannah, Georgia, February 8 - 12, 2009. AAS 09-153.
- [8] J. Simo and C. R. McInnes, "Solar Sail Orbits at the Earth-Moon Libration points," *Communications in Nonlinear Science and Numerical Simulation*, Vol. 14, No. 12, December 2009, pp. 4191–4196.
- [9] J. Simo and C. R. McInnes, "Designing Displaced Lunar Orbits Using Low-Thrust Propulsion," *Journal of Guidance, Control and Dynamics*, Vol. 33, No. 1, January-February 2010.
- [10] J. Simo and C. R. McInnes, "Displaced solar sail orbits: Dynamics and applications," *In 20th AAS/AIAA Space Flight Mechanics Meeting*, San Diego, California, February 14-17, 2010. AAS 10-222.
- [11] J. Simo and C. R. McInnes, "Tracking Unstable Periodic Orbits in the Circular Restricted Three-Body Problem," *Workshop on Applications on Control theory to Astrodynamics problems*, Surrey, England, April 26-27, 2010.
- [12] J. Simo and C. R. McInnes, "Feedback Stalization of Displaced Periodic Orbits: Application to Binary Asteroids," *Acta Astronautica*, Vol. 96, March-April 2014, pp. 106–115.
- [13] V. Szebehely, *Theory of Orbits: the restricted problem of three bodies*. New York and London: Academic Press, 1967.
- [14] A. E. Roy, *Orbital Motion*. Bristol and Philadelphia: Institute of Physics Publishing, 2005, pp. 118-122.
- [15] F. Vonbun, "'A Humminbird for the L₂ Lunar Libration Point'," *Nasa TN-D-4468*, April 1968.
- [16] R. Thurman and P. Worfolk, "The geometry of halo orbits in the circular restricted three-body problem," *Technical report GCG95, Geometry Center, University of Minnesota*, 1996.

- [17] G. Gómez, J. Llibre, R. Martínez, and C. Simó, *Dynamics and Mission Design Near Libration Points*, Vol. I, II. Singapore. New Jersey. London. Hong Kong: World Scientific Publishing Co. Pte. Ltd, 2001.
- [18] G. Gómez, A. Jorba, J. Masdemont, and C. Simó, *Dynamics and Mission Design Near Libration Points*, Vol. III, IV. Singapore. New Jersey. London. Hong Kong: World Scientific Publishing Co. Pte. Ltd, 2001.
- [19] R. Farquhar and A. Kamel, "Quasi-periodic orbits about the translunar libration point," *Celestial Mechanics*, Vol. 7, 1973, pp. 458–473.
- [20] R. Farquhar, "The utilization of Halo orbits in advanced lunar operations," *Nasa technical Note D-6365*, 1971.
- [21] J. Breakwell and J. Brown, "The 'halo' family of 3-dimensional periodic orbits in the Earth-Moon restricted 3-body problem," *Celestial Mechanics*, Vol. 20, 1979, pp. 389–404.
- [22] D. L. Richardson, "Halo orbit formulation for the ISEE-3 mission," *J. Guidance and Control*, Vol. 3, No. 6, 1980, pp. 543–548.
- [23] K. Howell, "Three-dimensional, periodic, 'halo' orbits," *Celestial Mechanics*, Vol. 32, 1984, pp. 53–71.
- [24] K. Howell and B. Marchand, "'Natural and Non-Natural Spacecraft Formations Near L_1 and L_2 Libration Points in the Sun-Earth/Moon Ephemerics System'," *Dynamical Systems: An International Journal*, Vol. 20, No. 1, March 2005, pp. 149–173.
- [25] S. Gong, J. Li, and J. Simo, "Orbital Motions of a Solar Sail around the L_2 Earth-Moon Libration Point," *Journal of Guidance, Control and Dynamics*, Vol. 37, No. 4, July–August 2014, pp. 1349–1356.
- [26] E. Battista, S. Dell'Agnello, G. Esposito, and J. Simo, "Quantum Effects on Lagrangian Points and Displaced Periodic Orbits in the Earth-Moon System," *Physical Review D*, Vol. 91, No. 8, April 2015, pp. 084041–1 – 084041–18.
- [27] E. Battista, S. Dell'Agnello, G. Esposito, L. Di Fiore, J. Simo, and A. Grado, "Earth-Moon Lagrangian Points as a Test Bed for General Relativity and Effective Field Theories of Gravity," *Physical Review D*, Vol. 92, No. 6, September 2015, pp. 064045–1 – 064045–21.
- [28] C. McInnes, "Solar sail Trajectories at the Lunar L_2 Lagrange Point," *J. of Spacecraft and Rocket*, Vol. 30, No. 6, 1993, pp. 782–784.
- [29] H. Baoyin and C. McInnes, "Solar sail halo orbits at the Sun-Earth artificial L_1 point," *Celestial Mechanics and Dynamical Astronomy*, Vol. 94, No. 2, 2006, pp. 155–171.
- [30] H. Baoyin and C. McInnes, "Solar sail equilibria in the elliptical restricted three-body problem," *Journal of Guidance, Control and Dynamics*, Vol. 29, No. 3, 2006, pp. 538–543.
- [31] H. Baoyin and C. McInnes, "Solar sail orbits at artificial Sun-Earth Lagrange points," *Journal of Guidance, Control and Dynamics*, Vol. 28, No. 6, 2005, pp. 1328–1331.
- [32] C. R. McInnes, "Artificial Lagrange points for a non-perfect solar sail," *Journal of Guidance, Control and Dynamics*, Vol. 22, No. 1, 1999, pp. 185–187.
- [33] S. Gong, J. Li, H. Baoyin, and J. Simo, "A New Solar Sail Orbit," *Science China Technological Sciences*, Vol. 55, No. 3, March 2012, pp. 848–855.
- [34] C. McInnes, A. McDonald, J. Simmons, and E. McDonald, "Solar sail parking in restricted three-body systems," *Journal of Guidance, Control and Dynamics*, Vol. 17, No. 2, 1994, pp. 399–406.
- [35] R. Farquhar, "The Control and Use of Libration-Point Satellites," *Ph.D. Dissertation, Stanford University*, 1968.
- [36] J.-J. E. Slotine and W. Li, *Applied Nonlinear Control*. Englewood Cliffs, New Jersey 07632: Prentice Hall, 1991.
- [37] S. Baig and C. McInnes, "Artificial Three-Body Equilibria for Hybrid Low-Thrust Propulsion," *Journal of Guidance, Control, and Dynamics*, Vol. 31, No. 6, November–December 2008, pp. 1644–1655.
- [38] M. Leipold and M. Götz, "Hybrid Photonic/Electric Propulsion," *Kayser-Threde, TR SOLA- TR-KTH-0001*, Munich, Jan. 2002, ESA Contract No. 15334/01/NL/PA.
- [39] G. Mengali and A. A. Quarta, "Trajectory Design with Hybrid Low-Thrust Propulsion system," *Journal of Guidance, Control, and Dynamics*, Vol. 30, No. 2, March–April 2007, pp. 419–426.
- [40] M. Ozimek, D. Grebow, and K. Howell, "Solar Sails and Lunar South Pole Coverage," *In AIAA/AAAS Astrodynamics Specialist Conference and Exhibit*, Honolulu, Hawaii, August 2008. Paper AIAA-2008-7080.